

Detecting the Rise and Fall of the First Stars by Their Impact on Cosmic Reionization

Kyungjin Ahn¹

Ilian T. Iliev²

Paul R. Shapiro³

Garrelt Mellema⁴

Jun Koda⁵
and

Yi Mao³

ABSTRACT

The intergalactic medium was reionized before redshift $z \sim 6$, most likely by starlight which escaped from early galaxies. The very first stars formed when hydrogen molecules (H_2) cooled gas inside the smallest galaxies, *minihalos* of mass between 10^5 and 10^8 solar masses. Although the very first stars began forming inside these minihalos before redshift $z \sim 40$, their contribution has, to date, been ignored in large-scale simulations of this cosmic reionization. Here we report results from the first reionization simulations to include these first stars and the radiative feedback that limited their formation, in a volume large enough to follow the crucial spatial variations that influenced the process and its observability. We show that reionization began much earlier *with* minihalo sources than without, and was greatly extended, which boosts the intergalactic electron-scattering optical depth and the large-angle polarization fluctuations of the cosmic microwave background significantly. Although within current *WMAP* uncertainties, this boost should be readily detectable by *Planck*. If reionization ended as late as $z_{\text{ov}} \lesssim 7$, as suggested by other observations, *Planck* will thereby see the signature of the first stars at high redshift, currently undetectable by any other probe.

Subject headings: cosmology: theory — galaxies: high-redshift — radiative transfer

¹Department of Earth Sciences, Chosun University, Gwangju 501-759, Korea; kjahn@chosun.ac.kr

²Astronomy Centre, Department of Physics & Astronomy, Pevensey II Building, University of Sussex, Falmer, Brighton BN1 9QH, United Kingdom

³Department of Astronomy, University of Texas, Austin, TX 78712-1083, U.S.A

⁴Department of Astronomy & Oskar Klein Centre,

Stockholm University, Albanova, SE-10691 Stockholm, Sweden

⁵Centre for Astrophysics & Supercomputing, Swinburne University of Technology, Hawthorn, Victoria 3122, Australia

1. Introduction

The theory of reionization has not yet advanced to the point of establishing unambiguously its timing and the relative contributions to it from galaxies of different masses. In a Cold Dark Matter (“CDM”) universe, these early galactic sources can be grouped broadly by their host dark-matter halo mass into two categories: minihalos (“MHs”) and “atomic-cooling” halos (“ACHs”). MHs have masses between $\sim 10^5$ and $\sim 10^8 M_\odot$ (solar masses) and virial temperatures below $\sim 10^4$ K, and thus molecular hydrogen (H_2) was necessary to cool the gas below this virial temperature to begin star formation. ACHs have masses above $\sim 10^8 M_\odot$ and virial temperatures $\gtrsim 10^4$ K, for which H-atom radiative line cooling alone was sufficient to support star formation. The ACHs can be split further into low-mass atomic-cooling halos (“LMACHs”; masses between $\sim 10^8$ and $\sim 10^9 M_\odot$), for which the gas pressure of the photoionization-heated intergalactic medium (“IGM”) in an ionized patch prevented the halo from capturing the gas it needed to form stars, and high-mass atomic-cooling halos (“HMACHs”; masses above $\sim 10^9 M_\odot$), for which gravity was strong enough to overcome this “Jeans-mass filter” and form stars even in the ionized patches.

Once starlight escaped from galactic halos into the IGM to reionize it, the ionized patches (“H II regions”) of the IGM became places in which star formation was suppressed in both MHs and LMACHs. At the same time, UV starlight at energies in the range 11.2 – 13.6 eV also escaped from the halos, capable of destroying the H_2 molecules inside MHs through Lyman-Werner band (“LW”) dissociation, even in the neutral zones of the IGM. This dissociation eventually prevented further star formation in some of the MHs where the background intensity was high enough.

In this letter we report the first radiative transfer simulations of reionization to include *all three* of the mass categories of reionization source halos, along with their radiative suppression, in a simulation volume large enough to capture both the global mean ionization history and the observable consequences of its evolving patchiness in a statistically meaningful way. We overcame the limitation of previous large-volume simulations by applying a newly developed sub-grid treatment to

include MH sources (section 2), and calculating the transfer of LW-band radiation self-consistently with the source population using the scheme of Ahn et al. (2009).

2. Methods

We performed a cosmological N-body simulation of structure formation with 3072^3 particles in a $114/h$ Mpc simulation box, using the WMAP5 background cosmology (Dunkley et al. 2009). For this we used the code CubeP³M (Merz et al. 2005; Iliev et al. 2008; J. Harnois-Deraps et al. 2012, in preparation), in which the gravity is computed by a P³M (particle-particle-particle-mesh) scheme. The simulation was started at redshift $z = 300$ and run to $z = 6$. N-body data (particle position and velocity) were recorded at 86 equally-spaced times (every 11.53 Myrs) from $z = 50$ to $z = 6$. Each data time-slice was then used to create matter density fields by smoothing the particle data adaptively onto a uniform mesh – or a “radiative transfer grid” – of 256^3 cells. All cosmological halos with masses $10^8 M_\odot$ or above (corresponding to 20 particles or more), and thus both LMACHs and HMACHs, were identified on-the-fly using a spherical overdensity halo finder with overdensity of $\Delta = 178$ with respect to the mean.

Unlike LMACHs and HMACHs, the MHs are too small to be resolved in our simulation box, and thus our radiative transfer grid was populated with MHs by means of a newly-developed sub-grid model, as follows. We started with a separate, high-resolution N-body simulation of structure formation in a comoving box with $(6.3/h \text{ Mpc})^3$ volume and 1728^3 particles, which resolved all MHs with mass $M \geq 10^5 M_\odot$ with 20 particles or more. We then partitioned the box into a uniform grid of 14^3 cells, such that each cell is the same size as one of the radiative transfer grid cells in our main, $114/h$ Mpc simulation box, and calculated the total number of MHs per cell and the cell density. Our results, shown in Fig. 1, indicate a strong and fairly tight correlation between the number of MHs located in a cell and its density. The best fit to this correlation at each redshift was then used to populate each grid cell in our $114/h$ Mpc box with MHs based on its density at each given time-slice.

Based on these structure formation results for

the IGM density field and the source dark matter halos, we then calculated the radiative transfer (RT) of H-ionizing and H₂-dissociating photons. The stars inside the ACHs are assumed to produce g_γ ionizing photons per baryon every 10 Myrs, where $g_\gamma \equiv f_\gamma/(t_\star/10 \text{ Myr})$, and where $f_\gamma \equiv f_e f_\star N_i$, f_e is the escape fraction of ionizing photons, f_\star is the star formation efficiency (i.e. the fraction of the halo baryonic mass which forms stars), and N_i is the number of ionizing photons per stellar baryon produced over the star's lifetime t_\star – we use $t_\star = 11.53 \text{ Myr}$ for both HMACHs and LMACHs, and $t_\star = 1.92 \text{ Myr}$ for MHs. We assign one Pop III star per MH, motivated by numerical simulations of first star formation inside MHs, which find that typically one Pop III star with a mass between 100 and 1000 M_\odot forms per MH in the absence of strong soft UV radiative feedback (Yoshida et al. 2006; Bromm et al. 2002; Abel et al. 2002). Star formation in MHs is suppressed when the local LW background – calculated at each time step in 3D using the scheme by Ahn et al. (2009), but now considering both ACHs and MHs and also improved in speed using the fast Fourier transform (FFT) scheme – reaches a certain threshold $J_{\text{LW, th}}$. At present the precise value of this threshold is not well determined, but the typical values found by high-resolution simulations of MH star formation are $J_{\text{LW, th}} = [0.01 - 0.1] \times 10^{-21} \text{ erg s}^{-1} \text{ cm}^{-2} \text{ sr}^{-1}$ (Machacek et al. 2001; Yoshida et al. 2003; O’Shea & Norman 2008). We adopted a constant value chosen from this range for each simulation.

The simulations with ACHs only (and without LW radiative transfer) are described in Iliev et al. (2012). Simulation parameters are given in Table 1.

3. Role of the first stars during cosmic reionization

We demonstrate the effects of the first stars by direct comparison of the results from two simulations, a fiducial case which includes all ionizing sources down to the first stars hosted by MHs (Case L2M1) and a corresponding reference case which includes the larger, atomically-cooling halos with exactly the same properties, but no MH sources (Case L2, previously presented in Iliev et al. 2012). Our results show that the early

reionization history is completely dominated by the first stars, while the late (redshift $z \lesssim 10$) history is driven by the stars inside HMACHs (Figs 2A and 2B, top panel). The very first stars start to form inside MHs at redshift $z \simeq 40$ (when the age of the universe was just 70 Myrs), and dominate the reionization process until $z \simeq 10$. Although the abundance of more massive halos, the ACHs, rises exponentially, they remain relatively rare, and thus sub-dominant, until $z \simeq 10$. After redshift $z \simeq 8$, though, the two reionization histories become largely indistinguishable, because the same HMACHs then dominate reionization. Before that, however, the mean intensity J_{LW} of the LW background produced by MH stars (see Fig. 2B, bottom panel) rises, on average, to $J_{\text{LW, th}}$, the threshold level above which H₂ is dissociated and star formation suppressed inside MHs, as early as $z \simeq 23$. Locally, $J_{\text{LW, th}}$ is reached even earlier, as early as $z \simeq 30$, due to inhomogeneities in the LW background. Thereafter, MH star formation continues but is self-regulated, which slows their contribution to reionization until the ACHs finally rise up to push J_{LW} above $J_{\text{LW, th}}$ (at $z \simeq 12$), halting MH star formation altogether, long before the MHs can complete reionization on their own.

Nonetheless, the MH sources (the first stars) can have quite a dramatic effect on the electron-scattering optical depth τ_{es} . While intergalactic H II regions fully overlap (at redshift z_{ov} , here defined as the epoch when the mean ionized fraction in the IGM by mass, x_m , first surpassed 99%) at almost identical redshifts, $z_{\text{ov}} \simeq 6.8$, with (L2M1) or without (L2) MHs, the early rise of x_m with MH sources boosts the optical depth by as much as 47% relative to that without MH sources: $\tau_{\text{es}} = 0.0861$ in case L2M1, while $\tau_{\text{es}} = 0.0603$ in case L2. This satisfies the current observational constraints on reionization: (1) reionization ended no earlier than redshift $z = 7$ (Fan et al. 2006; Ota et al. 2010; Mortlock et al. 2011; Bolton et al. 2011; Pentericci et al. 2011), and (2) $\tau_{\text{es}} = 0.088 \pm 0.015$ at 68% confidence level (Larson et al. 2011). Predicted values of τ_{es} and z_{ov} are model-dependent, and thus we tested the robustness of our conclusions by varying the physical parameters of MHs and ACHs (Fig. 3).

The first stars, born inside MHs, imprint a distinctive pattern on the global reionization history.

For example, in case L2M1, when the LW-plateau ended, reionization briefly stalled, since MHs no longer formed the stars which replenished the ionizing background and only ACH sources remained, thereafter; the ACH contribution took a bit more time to climb enough to move reionization forward again. This explains the brief “ x_m -plateau” from $z \sim 12$ to $z \sim 10$ in Fig. 2B for case L2M1, while in case L2, x_m grows continuously without showing such a plateau (Fig. 2B). This feature is generic (see Figs. 3 and 4B for different sets of parameters we explored). Reionization histories *without* MH sources, modelled either by large-scale radiative transfer simulations (Ciardi et al. 2003; Iliev et al. 2006, 2007; Trac & Cen 2007; McQuinn et al. 2007; Zahn et al. 2007; Iliev et al. 2012) or semi-analytical calculations (Haiman et al. 2000; Zahn et al. 2007), are all similar in that respect.

Reionization histories *with* MH sources, however, calculated here by large-scale N-body + radiative transfer simulations that take account of radiative suppression by both photoionization and LW dissociation, find an ionization plateau phase. Previous studies that considered MH stars and their impact were not able to settle the issue of their global effect on reionization. This is either because they simulated volumes much too small to represent a fair portion of the Universe (Ricotti et al. 2002; Yoshida et al. 2006; Ricotti et al. 2008), or else treated reionization by a semi-analytical, 1-zone, homogeneous approximation (either *with* LW suppression included (Haiman et al. 2000; Furlanetto & Loeb 2005) or *without* (Shapiro et al. 1994; Wyithe & Loeb 2003; Haiman & Bryan 2006; Wyithe & Cen 2007), which cannot capture its innate spatially inhomogeneous nature, or made a semi-analytical approximation that accounted statistically for spatial inhomogeneity but without LW suppression (Kramer et al. 2006).

We find that the global reionization history at $z \lesssim 20$ depends strongly on $J_{\text{LW, th}}$, and relatively weakly on $M_{\star, \text{III}}$. This is due to the very nature of self-regulation of the first star formation. The larger the $J_{\text{LW, th}}$ is, the weaker the suppression of star formation becomes, thereby temporarily hastening the progress of reionization. If the stellar mass $M_{\star, \text{III}}$ is smaller (Turk et al. 2009; Stacy et al. 2010; Greif et al. 2011a; Stacy et al. 2012) than those simulated here, those stars pro-

duce less ionizing and LW radiation and the resulting suppression is weaker, which partly compensates for the lower emission per star. Similar type of compensation would occur also when the number of MHs with a potential to form the first stars are smaller than our estimate, due to the relative offset of baryonic gas from some of the MHs (Tselikhovich & Hirata 2010; Greif et al. 2011b).

4. Probing the first stars with *Planck*

We thus conclude that the first stars hosted by MHs likely made an important contribution to reionization. But how can we probe them observationally? While significant, the effects of the first stars are largely confined to the early stages of reionization, at redshifts $z > 10$, which puts them beyond the reach of most current instruments. Future, very sensitive experiments such as the Square Kilometre Array (SKA) and the James Webb Space Telescope (JWST) may be able to probe these distant epochs directly. However, we have shown above that the combined effect of the first stars also considerably increases the value of τ_{es} compared to reionization scenarios in which the first stars are absent. Different values of τ_{es} are clearly reflected in the cosmic microwave background (CMB) polarization anisotropies at large scales. The current best constraints on τ_{es} by the *WMAP* satellite τ_{es} are still relatively weak, and thus models with low- τ_{es} values like L2 are still acceptable at the 2σ (95%) confidence level (Fig. 2B, middle panel). However, the *Planck* mission is currently measuring the CMB polarization far more precisely than *WMAP*, and from its results we should be able to discern the influence of the first stars on reionization. In Fig. 4A we show our forecasts for the angular spectra of CMB E-mode autocorrelation (EE).

As we discussed above, current observational constraints suggest that reionization was not complete before redshift $z \sim 7$. Imposing this condition as a prior on the allowed reionization histories $x_m(z)$, we predict that the *Planck* mission will clearly and unambiguously detect the era of first stars. In Fig. 4B we show a statistical measure of the *Planck* sensitivity to detecting the signature of the first stars through the principal component analysis by Hu & Holder (2003) and

Mortonson & Hu (2008)¹. Reionization principal components $\{S_\mu(z)\}$ are orthogonal, linearly independent eigen-vectors of the relevant Fisher matrix (evaluated with an arbitrarily chosen fiducial history $x_{e,\text{fid}}(z)$),

$$F_{ij} \equiv \sum_{l=2}^{l_{\text{max}}} \left(l + \frac{1}{2} \right) \frac{\partial^2 C_l^{\text{EE}}}{\partial x_e(z_i) \partial x_e(z_j)}, \quad (1)$$

which can be used to describe any generic ionization history $x_e(z)$ with just a small number of modes, such that

$$x_e(z) = x_{e,\text{fid}}(z) + \sum_{\mu=1}^{N_{\text{max}}} m_\mu S_\mu(z). \quad (2)$$

The mode amplitude m_μ , for a given history $x_e(z)$, becomes

$$m_\mu = \frac{\int_{z_{\text{min}}}^{z_{\text{max}}} dz S_\mu(z) [x_e(z) - x_{e,\text{fid}}(z)]}{z_{\text{max}} - z_{\text{min}}}. \quad (3)$$

Based on the *Planck* data after its full 2 years of planned operation, the narrow posterior distribution of allowed τ_{es} values will allow us to distinguish reionization models like L2 and L2M1 *unambiguously*, and thereby strongly constrain the available reionization parameter space. A high measured value of $\tau_{\text{es}} > 0.085$ will be a clear (if indirect) signature of the first stars.

Finally, we note that the presence of these first stars in cosmological MHs introduces the x_m -plateau noted above, which in turn imprints

characteristic features in the CMB polarization power spectrum. Hence, *Planck* might be able to distinguish (albeit at lower statistical significance, of $\gtrsim 2\sigma$ or $\gtrsim 95\%$) reionization models with and without first stars *even* if they have very similar values of τ_{es} and z_{ov} (Fig. 4B). Full reionization simulations like ours, in which constant mass-to-light ratios are assumed, find it hard to satisfy both of these observational constraints without including a significant contribution from the first stars, but some semi-analytical models (Haiman & Bryan 2006; Haardt & Madau 2012) do find such scenarios. However, all such models lack the plateau feature in the reionization history $x_m(z)$, and thus reside in a narrow window of m_μ -parameter space adjacent to that occupied by our no-MH cases, as demonstrated in Fig. 4B.

In summary, *Planck* is capable of distinguishing with high confidence between definitive classes of reionization scenarios allowed by the current constraints, and thereby significantly restricting the available parameter space. *Planck* will either probe the signature of the first stars, or show that the first stars had a negligible impact on reionization. Once these first results confirm the role of the first stars, simulations of the type presented here can be used to study other observable quantities and thus deepen our understanding of the early universe.

K.A. was supported in part by NRF grant funded by the Korean government MEST (No. 2009-0068141, 2009-0076868, 2012R1A1A1014646, 2012M4A2026720). ITI was supported by The Southeast Physics Network (SEPNet) and the Science and Technology Facilities Council grants ST/F002858/1 and ST/I000976/1. This study was supported in part by the Swedish Research Council grant 2009-4088, U.S. NSF grants AST-0708176 and AST-1009799, NASA grants NNX07AH09G, NNG04G177G and NNX11AE09G, and Chandra grant SAO TM8-9009X. The authors acknowledge the TeraGrid and the Texas Advanced Computing Center (TACC) at The University of Texas at Austin (URL: <http://www.tacc.utexas.edu>), and the Swedish National Infrastructure for Computing (SNIC) resources at HPC2N (Umeå, Sweden) for providing HPC and visualization resources that have contributed to the results reported within this paper. We acknowledge A. Lewis, A. Lid-

¹While we use the scheme developed by Mortonson & Hu (2008), we implemented the following ingredients in order to optimize the analysis for our purpose. First, to apply the late-reionization prior, $z_{\text{ov}} \leq 7$, we created 7 sets of principal components based on $x_{e,\text{fid}}(z) = \frac{40-z}{40-6.5}$ (see Eq. 2 for the definition of $x_{e,\text{fid}}(z)$), which make $x_e(z)$ behave well around $z \simeq z_{\text{ov}}$. We then used this late-reionization prior to reject any sample reionization history with $z_{\text{ov}} > 7$ when creating the Monte-Carlo Markov-chain of varying reionization models. Second, we improved the physicality condition of reionization history, or $0 \leq x_e(z) \leq 1$ at any z , which was somewhat poorly applied in Mortonson & Hu (2008). When a set of m_μ parameters (Eq. 3) were sampled during Markov-chain formation, we calculated the corresponding $x_e(z)$, and when either $\min(x_e(z)) > 0.04$ or $\max(x_e(z)) < 1.04$ was violated, we rejected that sample and searched for a new set of $\{m_\mu\}$. We allowed this small, 4% non-physicality in x_e because of the oscillatory nature of $x_e(z)$ coming from the limited number of principal components, which has only modest effects on the CMB E-mode polarization power spectrum C_l^{EE} .

dle and M. Mortonson for scientific and technical input on *Planck* forecasts (Lewis, Liddle) and COSMOMC modified for reionization principal components (Mortonson).

REFERENCES

- Abel, T., Bryan, G. L., & Norman, M. L. 2002, *Science*, 295, 93
- Ahn, K., Shapiro, P. R., Iliev, I. T., Mellema, G., & Pen, U. 2009, *Astrophys. J.*, 695, 1430
- Bolton, J. S., Haehnelt, M. G., Warren, S. J., Hewett, P. C., Mortlock, D. J., Venemans, B. P., McMahon, R. G., & Simpson, C. 2011, *Mon. Not. R. Astron. Soc.*, 416, L70
- Bromm, V., Coppi, P. S., & Larson, R. B. 2002, *Astrophys. J.*, 564, 23
- Ciardi, B., Stoehr, F., & White, S. D. M. 2003, *Mon. Not. R. Astron. Soc.*, 343, 1101
- Dunkley, J., et al. 2009, *Astrophys. J. Suppl.*, 180, 306
- Fan, X., & et al. 2006, *Astron. J.*, 132, 117
- Furlanetto, S. R., & Loeb, A. 2005, *Astrophys. J.*, 634, 1
- Greif, T. H., Springel, V., White, S. D. M., Glover, S. C. O., Clark, P. C., Smith, R. J., Klessen, R. S., & Bromm, V. 2011a, *Astrophys. J.*, 737, 75
- Greif, T. H., White, S. D. M., Klessen, R. S., & Springel, V. 2011b, *Astrophys. J.*, 736, 147
- Haardt, F., & Madau, P. 2012, *Astrophys. J.*, 746, 125
- Haiman, Z., Abel, T., & Rees, M. J. 2000, *Astrophys. J.*, 534, 11
- Haiman, Z., & Bryan, G. L. 2006, *Astrophys. J.*, 650, 7
- Hu, W., & Holder, G. P. 2003, *Phys. Rev. D*, 68, 023001
- Iliev, I. T., Mellema, G., Pen, U.-L., Merz, H., Shapiro, P. R., & Alvarez, M. A. 2006, *Mon. Not. R. Astron. Soc.*, 369, 1625
- Iliev, I. T., Mellema, G., Shapiro, P. R., & Pen, U. 2007, *Mon. Not. R. Astron. Soc.*, 376, 534
- Iliev, I. T., Mellema, G., Shapiro, P. R., Pen, U.-L., Mao, Y., Koda, J., & Ahn, K. 2012, *Mon. Not. R. Astron. Soc.*, in press (arXiv:1107.4772)

Table 1: Reionization simulation source halo properties and global history results. $M_{\text{III},*}$ and $J_{\text{LW,th}}$ are in units of solar mass (M_{\odot}) and $10^{-21} \text{ erg s}^{-1} \text{ cm}^{-2} \text{ sr}^{-1}$, respectively. *Note:* MH efficiencies $g_{\gamma, \text{MH}}$ ($f_{\gamma, \text{MH}}$) quoted here are for the minimum-mass halo assumed to contribute, $10^5 M_{\odot}$, which is roughly comparable to the average value for the MHs integrated over the halo mass function.

case	$g_{\gamma, \text{H}}$ ($f_{\gamma, \text{H}}$)	$g_{\gamma, \text{L}}$ ($f_{\gamma, \text{L}}$)	$g_{\gamma, \text{MH}}$ ($f_{\gamma, \text{MH}}$)	$M_{\text{III},*}$	$J_{\text{LW,th}}$	z_{ov}	τ_{es}	m_1, m_2, \dots, m_7
$g8.7_{\text{L130S}}$ (L1)	8.7 (10)	130 (150)	.	.	.	8.40	0.0841	-0.298, -0.0267, 0.289, 0.115, 0.0975, 0.0918, -0.0548
$g8.7_{\text{L130S}_M300_{J0.05}}$ (L1M1)	8.7 (10)	130 (150)	5063 (1013)	300	0.05	8.41	0.0934	-0.283, -0.0222, 0.268, 0.121, 0.0828, 0.0897, -0.0565
$g1.7_{\text{L8.7S}}$ (L2)	1.7 (2)	8.7 (10)	.	.	.	6.76	0.0603	-0.298, 0.00402, 0.372, 0.191, 0.0446, 0.0229, -0.0416
$g1.7_{\text{L8.7S}_M300_{J0.1}}$ (L2M1)	1.7 (2)	8.7 (10)	5063 (1013)	300	0.1	6.80	0.0861	-0.276, -0.00969, 0.302, 0.158, 0.0260, 0.00619, -0.0349

Iliev, I. T., Shapiro, P. R., Mellema, G., Merz, H., & Pen, U.-L. 2008, in Proceedings of the TeraGrid 2008 Conference. June 9-13, 2008. Las Vegas, USA, 31 (arXiv:0806.2887)

Kramer, R. H., Haiman, Z., & Oh, S. P. 2006, *Astrophys. J.*, 649, 570

Larson, D., et al. 2011, *Astrophys. J. Suppl. Ser.*, 192, 16

Machacek, M. E., Bryan, G. L., & Abel, T. 2001, *Astrophys. J.*, 548, 509

McQuinn, M., Lidz, A., Zahn, O., Dutta, S., Hernquist, L., & Zaldarriaga, M. 2007, *Mon. Not. R. Astron. Soc.*, 377, 1043

Merz, H., Pen, U.-L., & Trac, H. 2005, *New Astronomy*, 10, 393

Mortlock, D. J., et al. 2011, *Nature*, 474, 616

Mortonson, M. J., & Hu, W. 2008, *Astrophys. J.*, 672, 737

O’Shea, B. W., & Norman, M. L. 2008, *Astrophys. J.*, 673, 14

Ota, K., et al. 2010, *Astrophys. J.*, 722, 803

Pentericci, L., et al. 2011, *Astrophys. J.*, 743, 132

Ricotti, M., Gnedin, N. Y., & Shull, J. M. 2002, *Astrophys. J.*, 575, 33

—. 2008, *Astrophys. J.*, 685, 21

Shapiro, P. R., Giroux, M. L., & Babul, A. 1994, *Astrophys. J.*, 427, 25

Stacy, A., Greif, T. H., & Bromm, V. 2010, *Mon. Not. R. Astron. Soc.*, 403, 45

—. 2012, *Mon. Not. R. Astron. Soc.*, 422, 290

Trac, H., & Cen, R. 2007, *Astrophys. J.*, 671, 1

Tseliaxhovich, D., & Hirata, C. 2010, *Phys. Rev. D*, 82, 083520

Turk, M. J., Abel, T., & O’Shea, B. 2009, *Science*, 325, 601

Wyithe, J. S. B., & Cen, R. 2007, *Astrophys. J.*, 659, 890

Wyithe, J. S. B., & Loeb, A. 2003, *Astrophys. J. Lett.*, 588, L69

Yoshida, N., Abel, T., Hernquist, L., & Sugiyama, N. 2003, *Astrophys. J.*, 592, 645

Yoshida, N., Omukai, K., Hernquist, L., & Abel, T. 2006, *Astrophys. J.*, 652, 6

Zahn, O., Lidz, A., McQuinn, M., Dutta, S., Hernquist, L., Zaldarriaga, M., & Furlanetto, S. R. 2007, *Astrophys. J.*, 654, 12

This 2-column preprint was prepared with the AAS L^AT_EX macros v5.2.

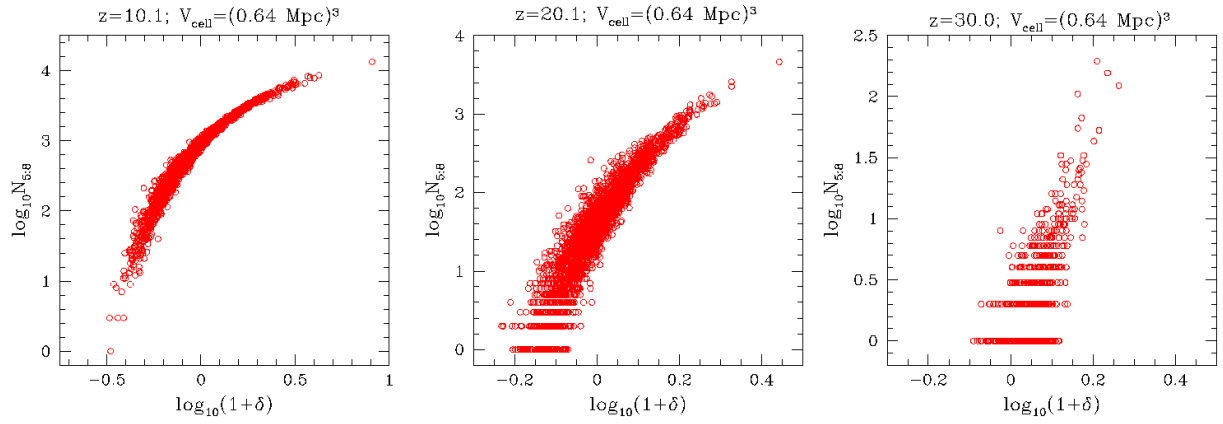


Fig. 1.— Correlation between the total number of MHs per RT cell ($N_{5.8}$) and the density of the RT cell in units of the mean density ($1 + \delta$), based on a $6.3/h$ Mpc box N-body simulation which resolves all halos with mass $M \geq 10^5 M_{\odot}$. Plots are for correlations at three different redshifts, $z = 30, 20.1$ and 10.1 from left to right. The volume of the RT cell is $(0.64 \text{ Mpc})^3$. The average correlation at each redshift was used to populate RT cells of the $114/h$ Mpc box with MHs at each redshift.

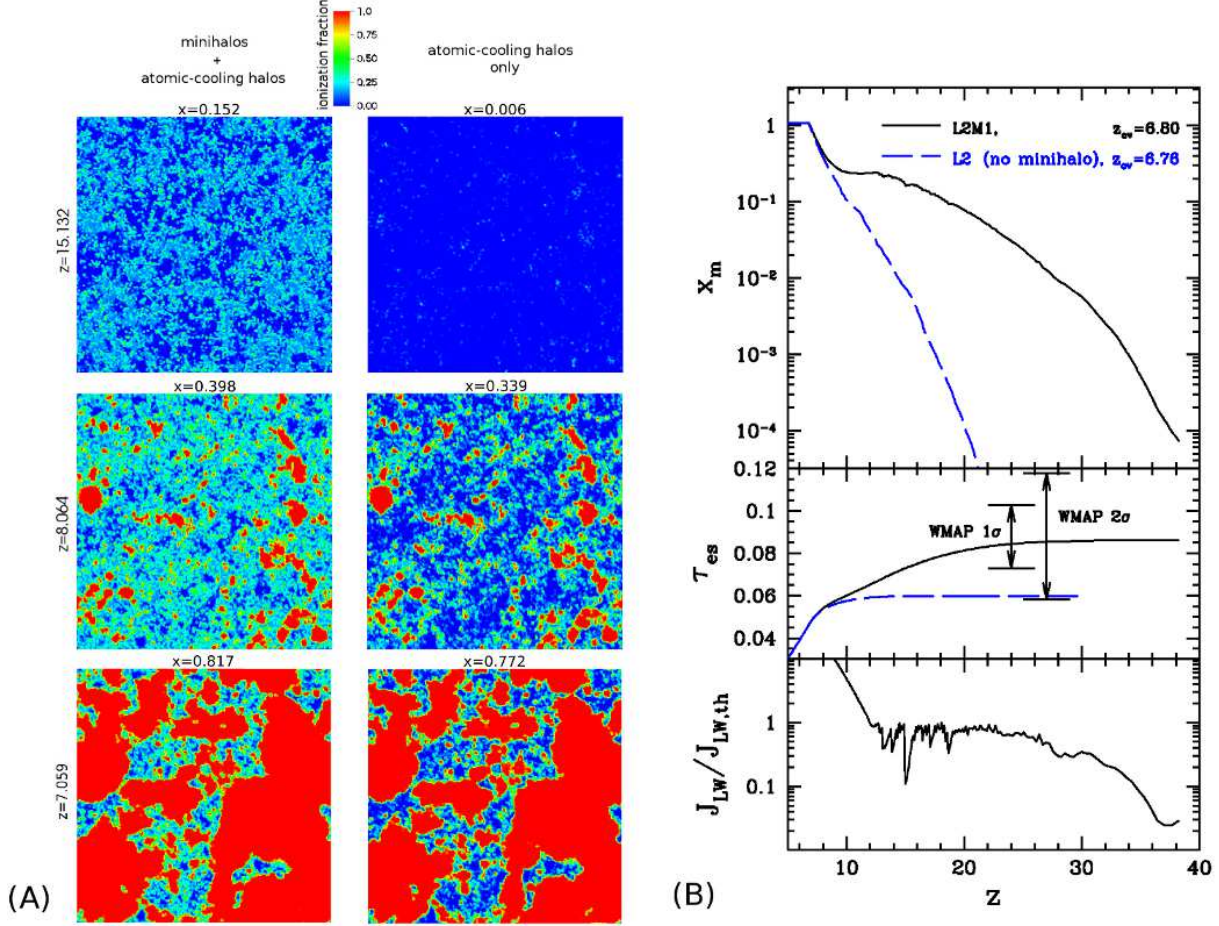


Fig. 2.— (A) Maps of evolving hydrogen-ionized fractions at different redshifts (rows), for our fiducial model with MH sources included, L2M1 (1st column), vs. the corresponding reference model with only atomically-cooling halos, case L2 (2nd column). The slices are $0.45/h$ Mpc-thick. Color represents linearly-scaled ionized fraction from 0 (blue) to 1 (red). (B) (top) Globally-averaged history of the mass-weighted ionized fraction for models L2M1 (black, solid) and L2 (blue, dashed). (middle) τ_{es} integrated from $z = 0$ to redshift z for L2 and L2M1. (bottom) Evolution of the mean J_{LW} in units of $J_{\text{LW,th}}$ for Case L2M1.

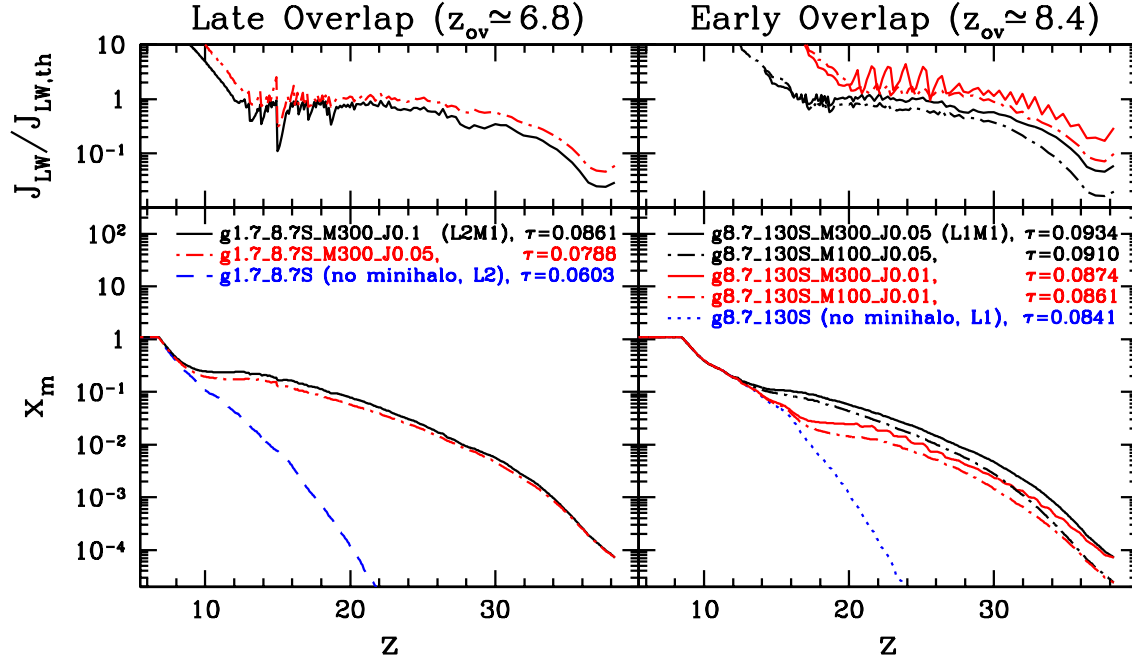


Fig. 3.— Model dependency of the history of cosmic reionization. In addition to cases L1 and L2, which do not account for MHs, we show predictions for MH-included cases by parametrizing the star formation inside MHs through $M_{*,\text{III}}$ (mass of the Pop III star) and $J_{\text{LW,th}}$ (threshold Lyman-Werner intensity). (Left) Late-overlap models. (Right) Early-overlap models.

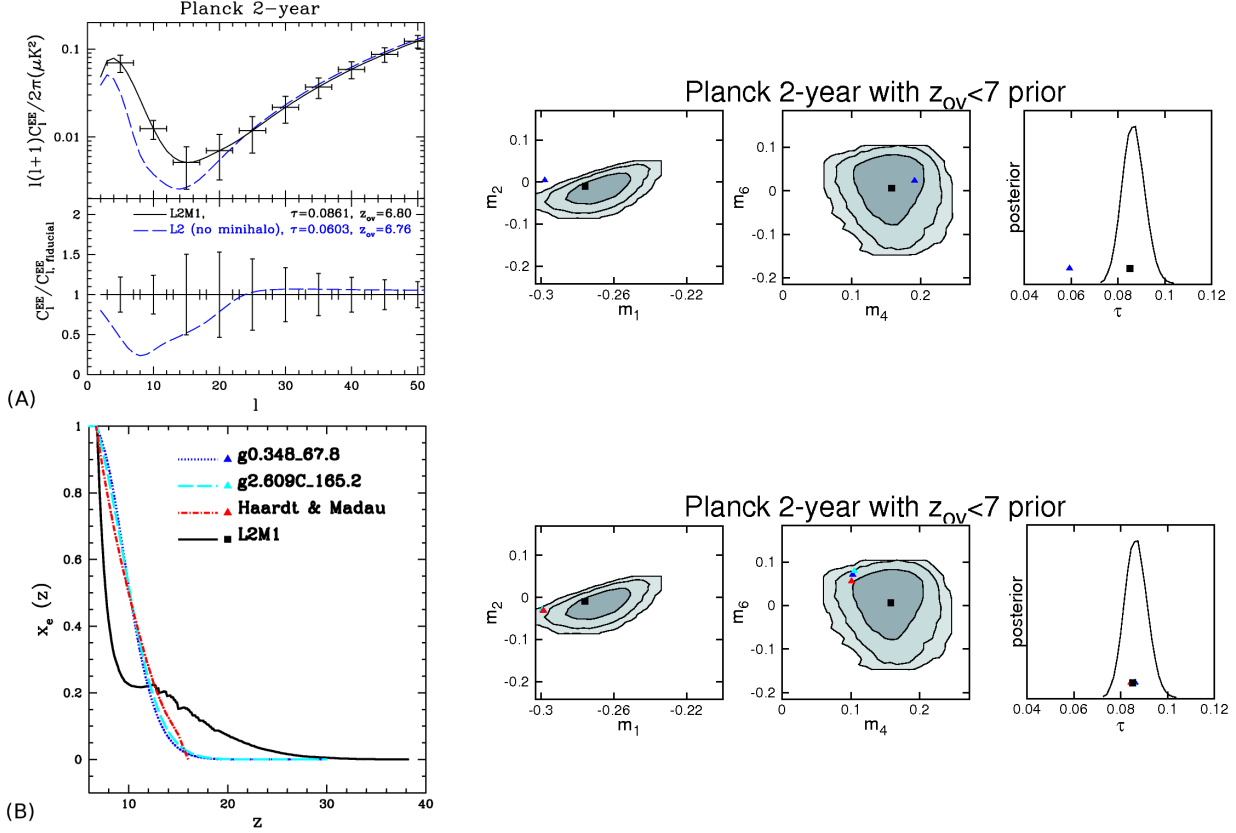


Fig. 4.— (A) Detecting the first stars. [left]: Forecasts of EE polarization power spectra of cases L2M1 (with MHs) and L2 (no MHs) for *Planck*. The error bars indicate the estimated *Planck* 2-year 1σ sensitivity including cosmic variance (top panel). [right]: Model-selection power of *Planck*. Contours represent 1σ (68%), 2σ (95%) and 3σ (99.7%) confidence levels from inside out, on marginalized posterior distributions of selected parameters (m_μ 's and τ_{es}) using mock data based upon Model L2M1 (black square). Case L2 (blue triangle) can be easily ruled out only from the measurement of τ_{es} by *Planck*. The prior condition of $z_{\text{ov}} \leq 7$ is applied here, which rules out early reionization ($z_{\text{ov}} \gtrsim 8$) models. (B) Breaking the degeneracy in z_{ov} and τ_{es} . [left]: Reionization histories of various reionization models, but with almost identical $z_{\text{ov}} (\simeq 6.8)$ and $\tau_{\text{es}} (\simeq 0.085)$. The model with MH sources (case L2M1, in black line) stands out from almost identical, no-MH models. $g0.348_67.8$ (no clumping; blue, dotted) and $g2.609C_165.2$ (with clumping; cyan, dashed) are semi-analytic models – note much larger, extreme ratios of $g_{\gamma, \text{L}}$ to $g_{\gamma, \text{H}}$ than those of cases L1(M1) and L2(M2) – obtained from equation (A1) of Iliev et al. (2007) with $n = 0.1$, and Haardt & Madau (red, dot-dashed) is from Haardt & Madau (2012). [right]: Hypothesis-testing power of *Planck* on MH-included (black square) vs. no-MH models (triangles). Contours have the same meaning as those in (A). No-MH models are clustered and well separated from case L2M1 at $\gtrsim 2\sigma$ confidence level. The same color scheme for model specification is used in left and right panels.